nature communications

Article

https://doi.org/10.1038/s41467-025-62883-8

Geometrically insensitive deform-and-go liquid crystal elastomer actuators through controlled radical diffusion

Received: 11 February 2025

Accepted: 30 July 2025

Published online: 14 August 2025

Check for updates

Xiaorui Zhou[1], Yi Sheng[1], Guancong Chen[1], Hong Wan[1], Luping Lu[1], Hao Xing[2], Jiacheng Huang[1], Zhan Zhu[1], Yufei Wang[1], Hanyuan Bao[1], Jingjun Wu[1], Qian Zhao[1], Tao Xie[1] & Ning Zheng[1]

The geometric shape and programming of mesogen alignment are two critical prerequisites for the effective actuation of liquid crystal elastomer (LCE) actuators. However, existing alignment programming approaches inevitably impose limitations on the geometric design of LCEs. In this study, we introduce a controlled radical diffusion mechanism that enables geometrically insensitive programming of actuation. Our findings show that LCEs can be deformed into complex structures via soft-elasticity and achieve the required mesogen alignment by simply soaking the LCE in an aqueous solvent of a free-radical initiator. The process requires no external assistance (maintained force, fixture, heating, or light) and the omnidirectional radicals' diffusion enables precise implementation of actuation across arbitrary geometries, including those produced through 3D printing, molding, embossing, and origami techniques. This "deform-and-go" strategy allows for scalable and versatile fabrication of advanced LCE actuators, representing a significant advancement in soft robotics engineering.

Soft actuators offer a broader range of actuation motion compared to rigid counterparts, owing to their significant advantages in terms of lightweight design, miniaturization, and user-friendliness[1–3]. As a result, they have garnered increasing attention in extensive applications such as biomedical[4], sensors[5], and environmental exploration[6]. Among various types of materials applicable for soft actuators, liquid crystal elastomers (LCEs) are particularly noteworthy due to their rapid response and high actuation strain[7–13]. Their special actuation behavior is determined by both geometric design and programming of mesogen alignment, with the former dictating their application scenarios while the latter governs their ability to undergo reversible actuation under external stimulation[14].

The precise alignment of mesogens therefore has become a fundamental requirement in the design and synthesis of LCEs[15]. Various strategies have been developed to achieve this, including surface anchoring interactions[16–18], electric/magnetic fields[19,20], shear extrusion[21–26], and mechanical stretching[27]. However, these methods encounter significant challenges when applied to intricate geometries due to their inherent reliance on specific shapes. Surface anchoring interactions provide an elegant approach for controlling alignment at the pixelated level but are limited to thin-film LCEs, as their effectiveness diminishes with increasing thickness. Electric and magnetic fields, while effective for inducing alignment, require sophisticated equipment and operate volumetrically, limiting their ability to achieve precise spatial control over complex geometries. Combining shear extrusion with direct ink printing offers the potential to fabricate intricate 3D shapes, but this method constrains the versatility of LCE actuation, as the shape and alignment are simultaneously determined during the fabrication process.

Mechanical stretching stands out as a particularly attractive approach due to its simplicity and broad applicability to most LCEs[28–30]. This technique typically requires an additional molecular

[1]State Key Laboratory of Chemical Engineering, College of Chemical and Biological Engineering, Zhejiang University, Hangzhou, China. [2]Hangzhou Zhijiang Advanced Material Co., Ltd, tests.711, Hangzhou, China. e-mail: zhengning@zju.edu.cn

fixation mechanism to stabilize the mesogen alignment[31–33]. A widely adopted method involves the two-stage curing protocol, where partially crosslinked gels[34] or polymers[35] containing unreacted functional groups are initially prepared, followed by complete curing through thermal or light exposure after stretching. In the case of thermal curing, LCEs must be heated above their nematic to isotropic phase transition temperature. At this stage, the material exhibits elastomeric behavior, requiring sustained external force to maintain alignment and prevent shape recovery. This necessity for mechanical fixtures throughout the stretching process limits its applicability to complex geometries. In contrast, light-induced crosslinking can utilize the soft elasticity of LCEs to fix temporary folded shapes without the need for fixtures. This soft elasticity arises from the robust π-π stacking interactions of reoriented mesogens during deformation. However, light-induced crosslinking encounters challenges in accessing shadow areas within complex 3D shapes. Other alignment-fixing mechanisms, such as dynamic bond exchange[36,37], crystallization[38], and solvent evaporation[39], also show promise. Yet, most of these methods require heating above the phase transition temperature for programming. An alternative, more elegant strategy involves inducing dynamic bond exchange at room temperature[40]. Nevertheless, this approach faces an inherent trade-off: achieving rapid and complete alignment fixation necessitates highly active dynamic bonds, which can compromise the stability of thermal-induced actuation. Consequently, developing a simple and universally applicable method for programming mesogen alignment that enables both geometric versatility and stable actuation in LCEs remains an unmet challenge.

A gentle alignment-fixing approach capable of achieving on-demand stable actuation for LCEs with arbitrary geometries is highly desirable. Most reported LCEs are synthesized through acrylate-thiol Michael addition and acrylate radical polymerization, where residual acrylate groups can undergo further crosslinked via radicals to fix the mesogen alignment[41]. We envision that if radicals could be generated at ambient temperatures without the need for heat or UV exposure, while maintaining the structural integrity of LCEs, the desired outcome can be attained. However, this presents significant challenges: the direct introduction of room-temperature initiators often compromises network stability, while solvent-mediated initiator introduction leads to undesirable swelling. Unexpectedly, we discovered that immersing LCEs in an ammonium persulfate (APS) aqueous solution enables the generated radicals to effectively permeate the LCEs. Simultaneously, the inherent hydrophobicity of LCEs prevents water-induced swelling, thereby preserving the deformed structure. Following this treatment, the LCE exhibits high stability and reversible actuation capabilities. This strategy is broadly applicable and holds substantial potential for the personalized customization and production of complex LCE actuators.

Results

The alignment fixing of LCE based on radical diffusion

Conventional alignment fixing methods generally rely on light or thermal stimuli, but they are limited by the presence of shadow areas and the requirement for continuous external force, respectively (Fig. 1a and detailed summary shown in Table S1). As such, the fabrication of intricate shapes of LCEs is constrained. In contrast, this work allows for the efficient construction of complex 3D structures that are unattainable by traditional alignment methods due to the unrestricted diffusion of free radicals. The specific programming procedure is illustrated in Fig. 1b, c. The as-cured LCE film can be cut into a "star" shape, which is well-suited for origami. Subsequently, this structure can be manually deformed into a "crane". To fix the shape and the orientation, the folded LCE is then placed in an aqueous solution containing 10 wt% APS. The sulfate radicals in the water can diffuse into the LCE network, initiating the radical polymerization of residual acrylates, as depicted by the chemical structures in Fig. 1d. Finally, the LCE exhibits a "crane"-like structure and reversible actuation in deformed regions.

The available LCE precursors, as depicted in Fig. 1e, encompass various liquid crystal monomers, chain extenders, and crosslinkers that can be utilized (more detailed information is shown in Table S2). These different systems can be polymerized through either thermal-induced Michael addition or photo-induced radical polymerization. We note that it is not necessary to precisely control both the composition and degree of polymerization in the system. Even a minimal amount of residual acrylate after complete polymerization can be utilized for subsequent shape and alignment fixing. In contrast, the alignment cannot be achieved in LCE systems lacking acrylate functional groups (Fig. S1). Hereafter, we first select a specific model system for investigation unless otherwise notified. The bis-[4-(6-acryloyloxyhexyloxy) benzoyloxy]−2-methylbenzene (RM82) is used as the liquid crystal monomer, combined with the chain extender 1,3-propanedithiol (EDDET) and the crosslinker pentaerythritol tetra(3-mercaptopropionate) (PETMP) in a 1:1 molar ratio of thiol to acrylate. The content of crosslinker is initially fixed at 20 wt%. The LCE can be obtained after being thermally cured under triethylamine catalysis. The swelling ratio of the LCE in different solvents is shown in Fig. S2, with a 1.6 wt% swelling ratio observed in water. The low swelling rate of LCE ensures its shape remains virtually unchanged in water, even after seven days (Fig. S3).

The characterization of alignment fixing mechanism

To verify the diffusion of sulfate radicals into the LCEs, we design a monitoring system as illustrated in Fig. 2a. The indicator consists of an acrylamide hydrogel containing xylenol orange sodium salt (XO) and Fe^{2+} ions for the detection of radicals. A 0.6 mm thick LCE film is placed on top of the hydrogel indicator, followed by a drop of APS aqueous solution on the LCE film. Over time, radicals generated from the APS solution can permeate through the LCE film and reach the surface of the hydrogel. These radicals will react with Fe^{2+} ions in the hydrogel, resulting in the transformation of Fe^{2+} to Fe^{3+} that triggers a color change reaction. Consequently, the initially orange XO changes into a purple complex, producing a visible purple spot on the orange hydrogel indicator. The results of the diffusion test are shown in Fig. 2b. To prevent the hydrogel from losing water, the radical monitoring system is placed in a controlled environment with a constant temperature of 15 °C and humidity of 90%. After 16 h, a faint purple spot can be observed, indicating that radicals have fully diffused through the LCE film. After 24 h, the obvious purple spot is visible on the hydrogel indicator. The hydrogel-based radical monitoring system confirms that the radicals could indeed diffuse into the LCE network.

As a well-known radical initiator, APS is widely used in the radical polymerization of hydrogels, most of which are composed of acrylic acid or acrylamide. To determine if the sulfate radicals produced by APS can induce chemical crosslinking for acrylate groups in the LCE network, we prepare a liquid crystal precursor containing RM82 and EDDET. Upon adding two drops of APS solution to the precursor, we observe clear gelation of the liquid crystal precursor after 1 min (Fig. 2c). Fourier-transform infrared (FTIR) spectroscopy results show that the characteristic infrared signals of residual acrylate groups in the prepared LCE (C-H bending at 811 cm^{-1}, C = C stretching at 1637 cm^{-1}) almost completely disappear after soaking in APS solution for 24 h (Fig. 2d, e). Amongst, the content of double bonds gradually decreases with the increase in soaking time (Fig. S4), indicating that the radicals generated by APS can induce reactions with residual acrylate groups. Differential scanning calorimetry (DSC) analysis shows that the diffusion of radicals has a negligible effect on the phase transition temperature of the LCE samples (Fig. S5). Furthermore, the mechanical properties of the LCE show slight changes (Fig. S6), with an increase in modulus attributed to the higher degree of crosslinking (Fig. S7).

https://doi.org/10.1038/s41467-025-62883-8

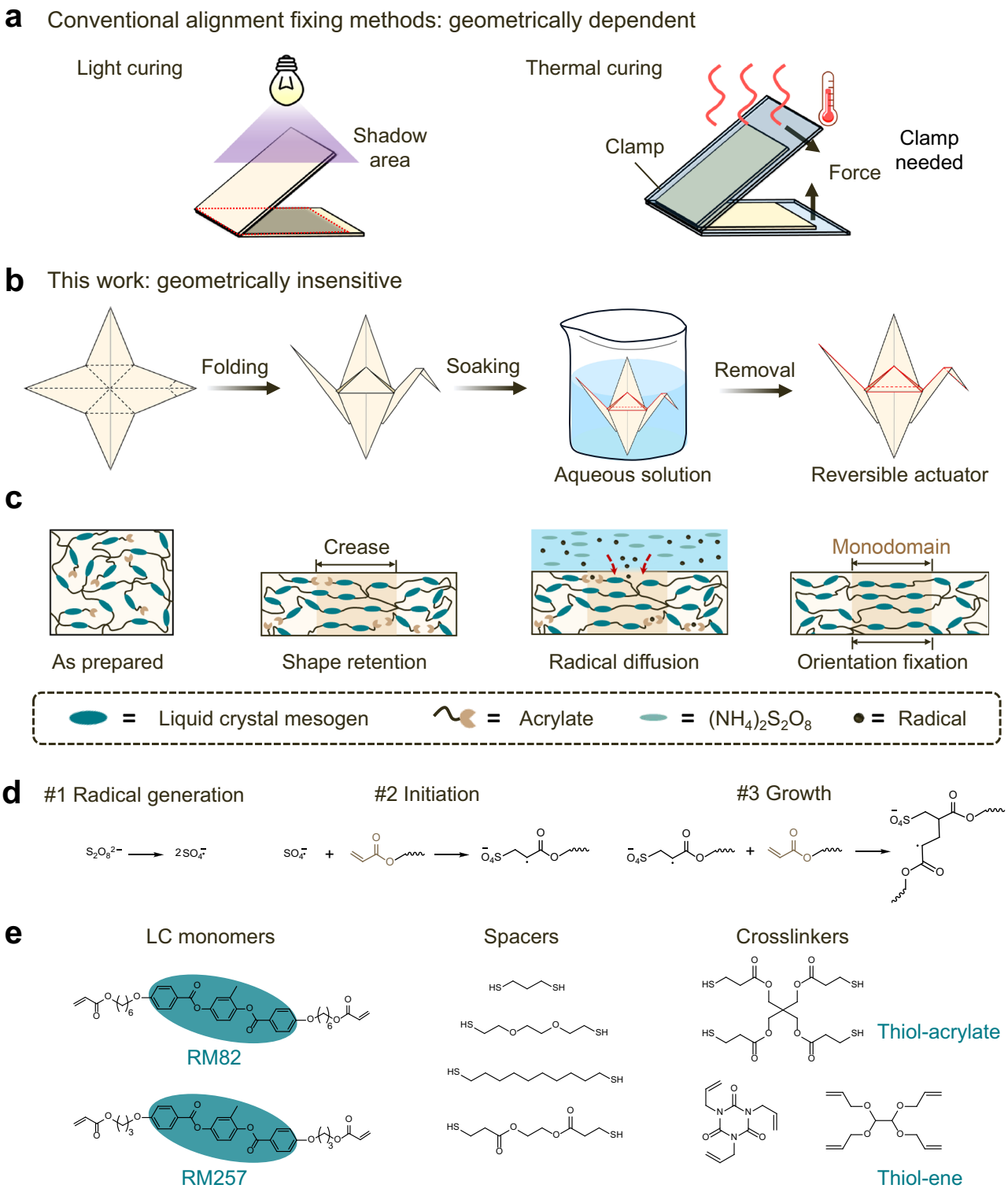

Fig. 1 | Alignment and actuation of LCEs enabled by radical diffusion. **a** Conventional alignment fixing methods. For the light curing method, as shown in the figure, the geometric structure creates shadow area where alignment fixation cannot be achieved. **b** The process for alignment fixing of this work through controlled radical diffusion. **c** The network illustration of the mechanism for mesogen alignment. **d** Chemical reaction structure formulae of acrylate free radical polymerization. **e** The available LCE compositions.

After confirming that radicals can diffuse into the LCE network and initiate the crosslinking of acrylate functional groups, we further investigate the diffusion kinetics and the underlying mechanisms driven by radical concentration gradients. Fig. S8–S10 indicate that as the sample thickness increases, the diffusion time correspondingly increases. The derivation and calculation results (see Supplementary Information) are consistent with Fick's law, indicating that the time required for complete diffusion is proportional to the square of the sample thickness, with an apparent diffusion coefficient of 1.41×10^{-4} $m^2 \cdot s^{-1}$.

https://doi.org/10.1038/s41467-025-62883-8

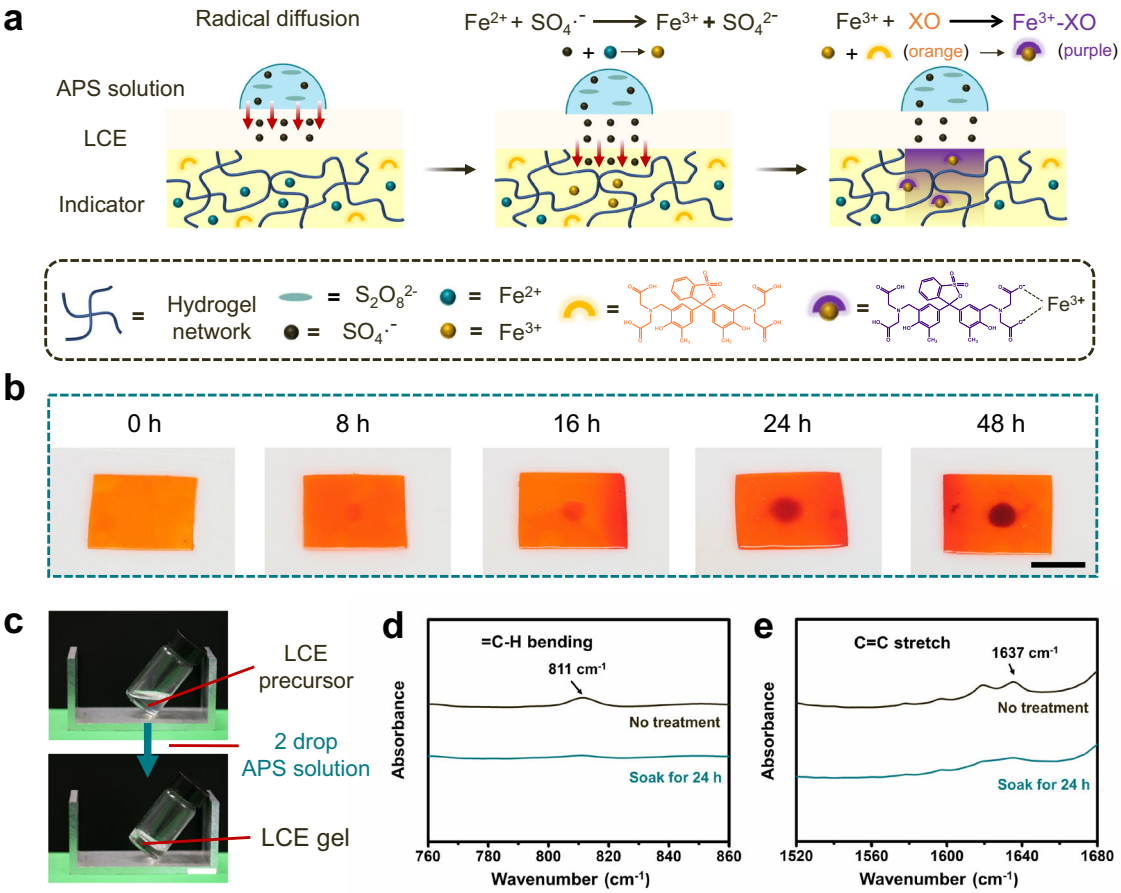

Fig. 2 | The mechanism of radical diffusion and reaction. a The schematic illustration of the radical diffusion monitoring process. The indicator caused the color of the gel to change from orange to purple upon contact with iron ions. **b** The results of radical diffusion. **c** The changes in the LCE precursor before and after adding the APS solution. LCE precursor is composed of 1 g of RM82 and an equimolar amount of EDDET dissolved in 1 g of N, N′-dimethylformamide. **d**, **e** FTIR spectroscopy of LCE film before and after soaking in APS solution. All scale bars are 1 cm.

The actuation performance of LCE actuator fabricated through radical diffusion

We hereafter investigate the actuation performance of the LCE. As shown in Fig. 3a, the uniaxially stretched LCE film (with a pre-stretched strain of 120%) exhibits nearly 110% reversible strain after soaking in APS aqueous solution for 24 h. In contrast, the same LCE film soaked in deionized water shows no actuation capability. This further confirms that the reversible actuation of the LCE originated from the diffusion of radicals generated by APS. The chemically crosslinked nature of our LCEs ensures high actuation stability even at elevated temperatures up to 140 °C (Fig. 3b, more heating-cooling cycles are shown in Fig. S11), which is in stark contrast to the limited stability observed in LCEs fixed through dynamic bond exchange. To ensure long-term thermal stability, the LCE samples are subjected to thermal treatment at 140 °C for 72 h (Fig. S12). The actuation strain shows only a minor change, decreasing from 106 to 100%. In addition, the actuation performance of samples stored for approximately one year is assessed (Fig. S13, S14), revealing negligible changes in their behavior and thereby confirming the storage stability of the LCEs. Typically, the initially prepared LCE films are isotropic, as confirmed by the two-dimensional wide-angle X-ray diffraction (WAXD), which shows a uniform ring (Fig. 3c). After stretching and soaking, two distinct arcs are observed in the WAXD, indicating that the reversible actuation of LCE films originates from the anisotropy generated in the network. This is further supported by polarized optical microscopy images (Fig. 3d), which show alignment consistent with the direction of the applied pre-stretching.

Several factors would affect the actuation behaviors during the programming. It can be estimated by the actuation strain, with the definition shown in the Experimental Section. We select an LCE film with a length of 20 mm, a width of 4 mm, and a thickness of 0.6 mm as the test sample. Since the crosslinking process of the LCE is highly dependent on radical diffusion, we first explore the correlation between APS concentration, soaking time, and the resulting actuation strain with the same pre-stretch strain of 100%. As illustrated in Fig. 3e, the actuation strain of the LCE sample progressively increases with soaking time until it reaches a plateau. It is evident that at low APS concentrations, the fixing effect on the alignment of mesogens is positively correlated with the concentration of APS. This indicates that achieving the same actuation strain requires longer soaking times in lower concentration APS solutions. However, we found that when the APS concentration exceeds 24%, the solution loses its ability to effectively fix the alignment. This is because APS tends to decompose and produce oxygen at high concentrations, reducing the efficiency of radical generation. It can be supported by the observation of noticeable bubble formation in high-concentration APS solutions. The optimal orientation fixing effect is achieved when the LCE sample is soaked in a 4 wt% APS solution. Therefore, this soaking condition is used for subsequent investigations. In addition, at this concentration, the minimal oxidizing property of APS does not lead to any degradation in the actuation performance or mechanical properties of the LCE

https://doi.org/10.1038/s41467-025-62883-8

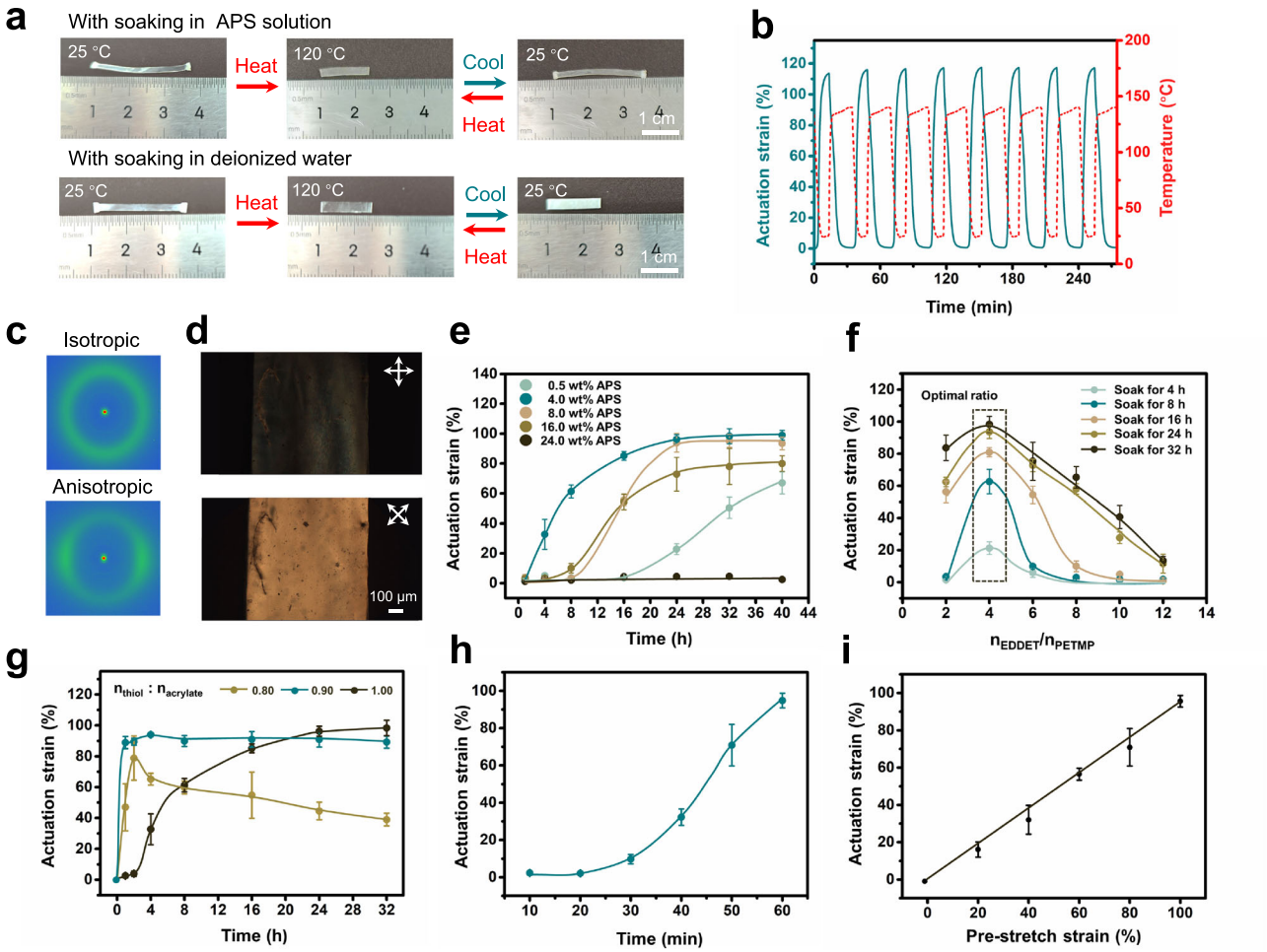

Fig. 3 | The actuation performance of LCE. a The results of LCEs soaked in APS solution and deionized water. **b** Cyclic actuation behavior of the LCE sample upon heating and cooling. **c** WAXD patterns before and after the programming. **d** Polarized optical micrographs of aligned LCE. **e** The relationship between actuation strain, APS concentration, and soaking time. **f** The dependence of actuation strain on the crosslinker content and soaking time. **g** The effect of residual acrylate content on the actuation strain. **h** The dependence of actuation strain on the soaking time. **i** The relationship between actuation strain and pre-stretch strain. The sample in (**h**) and (**i**) exhibits a 4:1 ratio of EDDET to PETMP, while the molar ratio of acrylate to thiol is maintained at 1:1. All error bars correspond to the s.d. ($n = 3$).

(Fig. S15, S16). This observation is consistent with the FTIR results, which indicate that the material's characteristic peaks remain virtually unchanged after 48 h of soaking (Fig. S17).

The alignment fixing effect is also influenced by the LCE network composition. As shown in Fig. 3f, both excessively high and low crosslinking densities (i.e., the molar ratio between the chain extender EDDET and crosslinker PETMP) are detrimental to the mesogen alignment fixing. This phenomenon may be attributed to the fact that a high crosslinking density hinders the diffusion of free radicals, whereas a low crosslinking density results in excessive spacing between residual acrylate groups, leading to unfavorable chemical crosslinking. Consequently, there is an optimal crosslinker ratio for this thermally polymerized LCE network, specifically when the chain extender EDDET to crosslinker PETMP ratio is 4.

To simplify the initial preparation of the LCE network, we have fixed the molar ratio of acrylate to thiol at 1:1, thereby enabling APS-initiated chemical crosslinking to occur among the few remaining acrylate groups. This leads us to question whether a substantial presence of acrylate functional groups in the network could significantly enhance the efficiency of alignment, thereby reducing the soaking time needed to reach maximum actuation strain. Indeed, as shown in Fig. 3g, the efficiency of alignment fixing is much higher when the acrylate is in excess (i.e., the molar ratio between acrylate and thiol is 1:0.9). The maximum strain is reached after 1 h of soaking in the APS solution. When the acrylate content is further increased (i.e., the acrylate to thiol molar ratio is 1:0.8), alignment fixing could still be completed in a short time, but the actuation strain decreases with prolonged soaking. This decrease is due to excessive chemical crosslinking which would restrict the actuation of LCE. The observed slight enhancement in the mechanical properties of the LCE samples after soaking can be attributed to an increase in the crosslinking density of the material resulting from the crosslinking of residual acrylate functional groups. Additionally, the actuation strain of the optimized LCE sample increases with the increase of soaking time and the pre-stretched strain (Fig. 3h, i). After soaking for one hour, the LCE sample achieved 100% actuation strain. We expand the range of water-soluble free radical initiators for generating the necessary radicals (Fig. S18), and it is observed that nearly all the selected radical initiators can achieve effective liquid crystal mesogen alignment fixing, but APS provided the best results.

The fabrication of LCE 3D structure

The arbitrary spatial diffusion of free radicals allows us to impart actuation capabilities in a diverse range of 3D structures. Digital light processing (DLP) 3D printing offers a flexible method for custom forming 3D structures of LCE. This printing method typically exhibits

https://doi.org/10.1038/s41467-025-62883-8

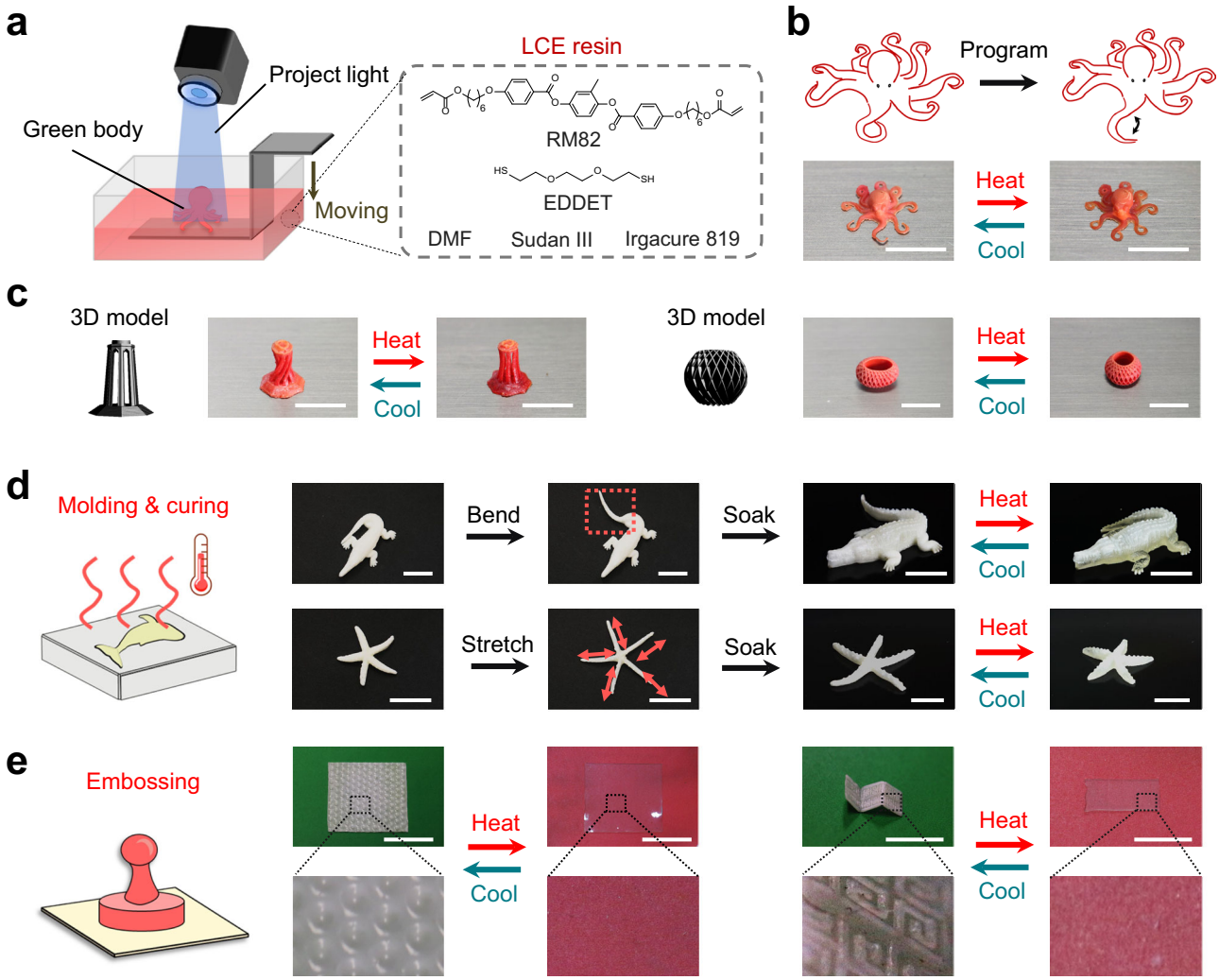

Fig. 4 | The manufacture and alignment programming of LCE 3D structure. **a** DLP 3D printing setup and LCE resin formulation. **b** The programming illustration and actuation behavior of 3D printed octopus. **c** The 3D printed LCE objects and corresponding reversible actuation. For all samples, the soaking time is controlled at 24 h. **d** Fabricating 3D structure through molding. The arrow represents the direction of the stretching. The soaking time is controlled at 24 h. **e** Forming reversible visual patterns through the embossing technique. The soaking time is controlled at 4 h and the thickness of LCE films is 0.6 mm. All the scale bars are 1 cm.

enhanced printing speed and heightened printing accuracy compared with typical direct ink writing (DIW). The liquid crystal precursors for DLP 3D printing are commonly cured in an isotropic state. Therefore, directly printed structures lack actuation capability and usually require post alignment to impart actuation to the 3D structures, such as crystalline[38] or solvent evaporation[39]. The actuation stability achieved by these methods is not as good as that of chemical crosslinking. As shown in Fig. 4a, we select commonly used photo-curable LCE precursors for DLP 3D printing. It is worth noting that despite the utilization of radical polymerization in both DLP 3D printing and our alignment programming technique, these two processes do not interfere with each other. The printed complex 3D models exhibited stable thermal responsive reversible actuation after programming (Fig. 4b, c, Movie S1), demonstrating the applicability of this method to 3D printing.

Additionally, 3D structures can also be achieved through molding by utilizing thermal curing LCE systems, as outlined in Table S1. Complex structures like a “crocodile” and a “starfish” can be molded and programmed to achieve the actuation (Fig. 4d, Movie S2). Embossing technology offers a versatile approach to customizing arbitrary visual patterns on LCE films. When subjected to applied pressure, the thickness of the LCE material undergoes alteration, resulting in orientation in these domains (Fig. S19). After fixing, these patterns exhibit a reversible transition between visible and invisible states (Fig. 4e and S20). This method further enables the embossing of complex patterns onto 3D macroscopic shapes formed by folding. Notably, the shape transitions in multiscale occur independently, a capability that is challenging to achieve with other alignment methods. Other techniques, such as kirigami, can also be employed. The locally cut LCE 2D sheet can transform into 3D shapes under external tensile forces. After programming, the kirigami structures possess the ability to reversibly transform back into 2D shapes (Fig. S21).

The fabrication of LCE origami

Origami is a traditional art form that creates beautiful 3D structures by folding paper into various shapes and patterns[42]. It is not only an artistic expression but also has found widespread application in fields such as structural design and mechanical engineering, including foldable architectural structures[43], medical devices[44], and shape-morphing soft robots[45]. LCE films can be utilized as origami materials to fabricate various 3D structures with reversible actuation, offering numerous potential functions. The early application of origami techniques in the preparation of LCEs is primarily observed in dynamic chemistry systems[46]. However, these bond exchanges are either induced by

https://doi.org/10.1038/s41467-025-62883-8

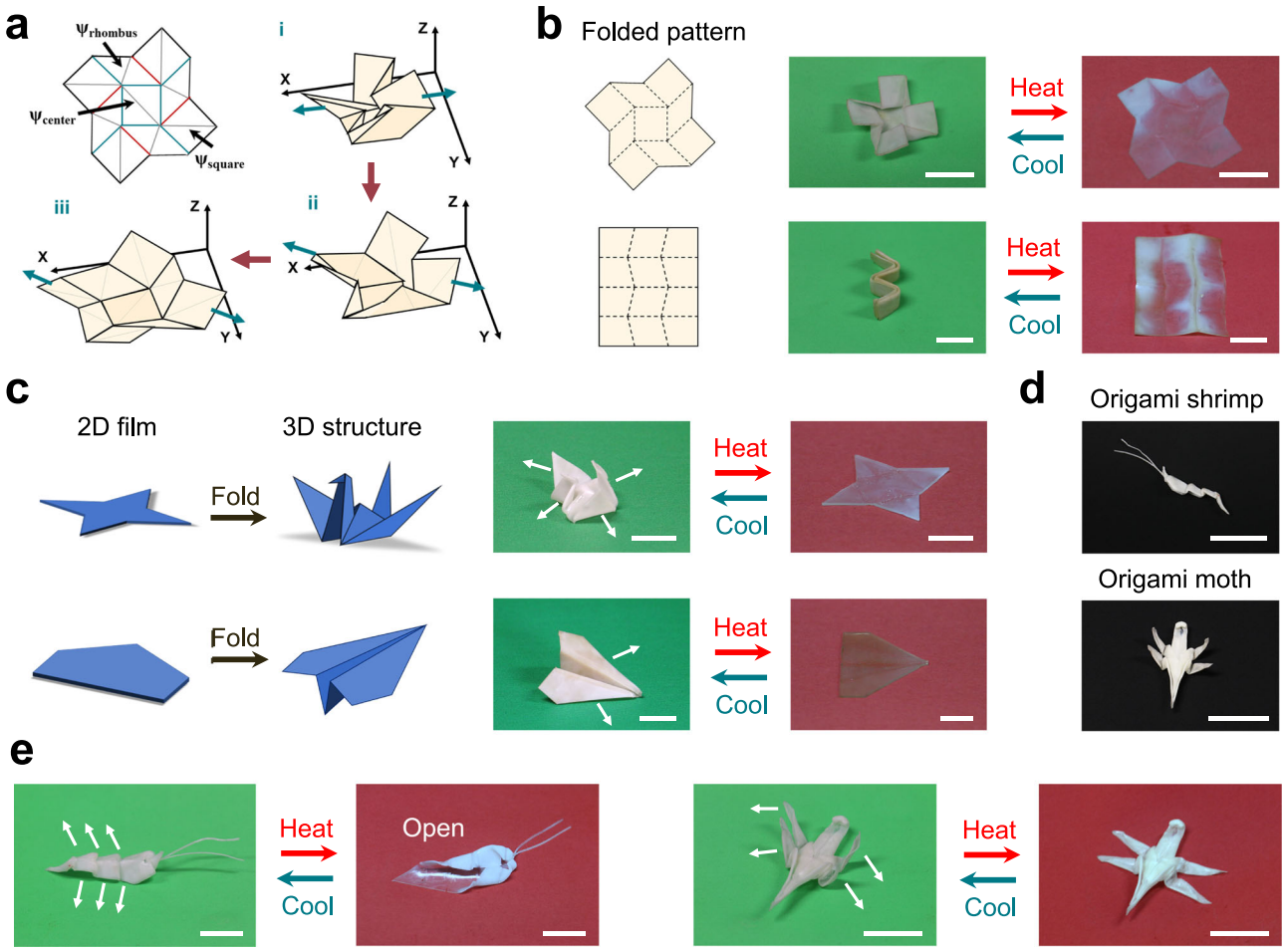

Fig. 5 | LCE origami. a Folding and unfolding process of Square-Twist origami consisting of square and rhombus panels. **b** Design and actuation behaviors of different origami patterns. **c** 2D to 3D reversible transformation examples of origami "crane" and "airplane". **d** The origami LCE "shrimp" and "moth" obtained through multiple folds. **e** 3D to 3D reversible transformation examples of origami "shrimp" and "moth". The white arrows in (**c**, **e**) represent their actuation directions. All the scale bars are 1 cm.

thermal or light stimuli during the alignment process, which imposes limitations on fabricating intricate shapes as depicted in Fig. 1a. In contrast, our LCEs can be easily folded or crumpled into origami structures at room temperature, without exhibiting the typical elastic rebound observed in conventional elastomers. This enables us to effortlessly fabricate origami LCEs.

Among various origami patterns, Square-Twist origami represents a type with fourfold rotational symmetry (Fig. 5a). Its folding pattern consists of alternating squares and rhombus panels, where the internal edges are all either mountain or valley creases (Fig. S22). An analysis of the geometric constraints reveals that the crease pattern has zero degrees of freedom (DOF) and therefore it should not be foldable (see Supplementary Information). However, based on the fact that real materials can be folded, this origami pattern can be achieved by exploiting the bending deformation not explicitly indicated in the crease, thereby providing additional DOF[47]. The bending DOF of these hidden panels generates an energy barrier. By releasing the bending DOF, the non-rigid foldable Square-Twist origami structure stores elastic energy, primarily in the form of bending energy in the panels and folding energy at the creases during the folding/unfolding process. We perform an energy analysis on the Square-Twist LCE origami (detailed information is provided in the Supplementary Information). The results show that the bending-to-crease energy ratio (k_b/k_c) of our LCE is 0.6. For $k_b/k_c \leq 1$, the geometric configuration of the material formed through folding is stable and will not readily deform under unstimulated conditions[47]. Furthermore, during the unfolding and folding processes, the additional DOF provided by $k_b/k_c \leq 1$ helps eliminate the hysteresis behavior caused by changes in the stable state. This strongly demonstrates the good compatibility of LCEs with this origami structure. We therefore fold LCE films according to the Square-Twist pattern, this structure demonstrates the expected reversible expansion and contraction upon heating and cooling after programming (Fig. 5b, Movie S3). Additionally, we fabricate reversible deployable structures formed using other folding patterns. These types of non-rigid foldable origami structures hold promise for designing mechanical energy storage devices and deployable spacecraft structures.

Beyond deployable structures, we also demonstrated classic origami based on paper folding. As shown in Fig. 5c, the origami "crane" and origami "airplane" can revert to 2D sheets when heated above the nematic-isotropic transition temperature, and they can reversibly return to their folded 3D shapes upon cooling (as shown in Movie S4). These two types of foldable structures share a similar folding mechanism with the deployable folding pattern, exhibiting a reversible transformation from 2D to 3D shapes. The diffusion mechanism of radicals allows for alignment locking at any crease, enabling us to design LCEs into complex and diverse artistic structures. As demonstrated in Fig. 5d, LCEs are folded multiple times to form structures

resembling "shrimp" and "moths". Due to the interlocking of the origami structures and the thermal conduction effects, these 3D structures can undergo local deformation upon heating, demonstrating a reversible transformation from one 3D shape to another 3D shape (Fig. 5e, Movie S5). The attainment of these intricate 3D origami structures is beyond the capabilities of currently reported programming methods.

Discussion

In summary, we have discovered an LCE programming mechanism through radical diffusion-induced chemical crosslinking in aqueous conditions. This strategy can effectively fix the mesogen alignment and impart actuation capability of LCEs, maintaining their macroscopic structural integrity. The resulting actuation strain exhibits a high magnitude and demonstrates exceptional stability in actuation. By applying localized external forces, regionally controlled and customized alignment patterns can be designed, thereby endowing LCEs with spatially controlled actuation behaviors. The geometric insensitivity of the radical diffusion enables the creation of intricate 3D structures by integrating molding, embossing, and kirigami strategies, in conjunction with the utilization of DLP 3D printing to achieve highly complex designs. In addition, the maintained soft elasticity of LCEs allows them to be deformed into various foldable and deployable structures, akin to the art of origami. Theoretically, by spatiotemporally controlling the alignment of mesogens through strategies such as regulating the kinetics of radical diffusion and designing heterogeneous network structures, it is possible to further enhance the complexity of LCE actuation. This represents a promising research direction for future investigation. We further note that the use of the APS solution may raise concerns regarding waste disposal and environmental impact. Therefore, in industrial production, eco-friendly initiators hydrogen peroxide solutions, can be used as a substitute, which are also capable of achieving effective alignment fixation. To ensure the stability of this method for large-scale production, both the soaking time and the initiator concentration should be carefully controlled. A sufficiently long soaking time, along with real-time monitoring of initiator consumption and timely replenishment, can help ensure consistent alignment performance. Our approach is broadly applicable to most acrylate LCE systems and facilitates large-scale programming of actuators and soft robots.

Methods

Materials

The liquid crystal mesogen with terminated acrylate groups 1,4-bis-[4-(6-acryloyloxy-hexyloxy) benzoyloxy]−2-methylbenzene (RM82, purity: 97%) and 1,4-bis-[4-(3-acryloyloxypropyloxy) benzoyloxy]−2-methylbenzene (RM257, purity: 97%), epoxy liquid crystal mesogen 4,4′-bis(2,3-epoxypropoxy)biphenyl (purity: 98%) were purchased from Beijing Bayi Space LCD Technology Co., Ltd. The 2,2′-(ethylenedioxy) diethanethiol (EDDET, purity: 97%), glycol di(3-mercaptopropionate) (purity: 99%), acrylamide (AAm, purity: 99%), tetrakis(allyloxy)ethane (purity: 99%), and sebacic acid (purity: 99%) were obtained from Sigma-Aldrich. The pentaerythritol tetra(3-mercaptopropionate) (PETMP, purity: 95%) was procured from Rhawn. 2,2-dimethoxy-2-phenylacetophenone (DMPA, purity: 98%), triazobicyclodecene (TBD, purity: 98%), 1,8-diazabicyclo[5.4.0]undec-7-ene (DBU, purity: 99%), ammonium persulphateand (APS, purity: 99%), 1,3-dimercaptopropane (purity: 98%), 1,10-decanedithiol (purity: 96%), ferrous sulfate (purity: 99%) and 1,3,5-triallyl-1,3,5-triazine-2,4,6(1H,3H,5H)-trione (purity: 98%) were purchased from TCI. The N,N′-methylene diacrylamide (purity: 98%), xylenol orange sodium salt (XO, purity: 99%), hydrochloric acid, 2,2′-azobis[2-(imidazolin-2-yl)propane] dihydrochloride (purity: 98%), and triethylamine (TEA, purity: 99%) were purchased from Macklin. The photo-initiator Irgacure 2959 (purity: 98%) was obtained from Aladin. All the chemicals were used as received.

Synthesis of LCE samples through Michael-addition

Taking the selection of EDDET as the chain extender as an example, the synthesis of the LCE network via Michael addition was demonstrated. For systems employing different chain extenders, equimolar amounts of thiol and liquid crystal monomer were used, while maintaining a fixed molar ratio of chain extender to crosslinker at 4. In the case of the LCE system with an n_{EDDET}/n_{PETMP} ratio of 4, where the molar amounts of thiol and acrylate were kept equivalent, the synthesis was carried out as follows: RM257 (1 g), EDDET (0.2063 g), and PETMP (0.1382 g) were dissolved in DMF (1 g) at 80 °C. Subsequently, 0.05 g of triethylamine (TEA) was added to the mixture. After thorough mixing and degassing, the solution was cast between two glass slides separated by a silicone rubber spacer and cured in an oven at 80 °C for 12 h. Upon completion of the reaction, the resulting sample was dried in a vacuum oven at 70 °C for 12 h to completely remove residual DMF and TEA.

Synthesis of LCE samples through radical polymerization

Taking tetrakis(allyloxy)ethane as the crosslinker as an example, the synthesis of the LCE network via radical polymerization was demonstrated. For systems employing different crosslinkers, the molar ratio of thiol to acrylate was maintained at 1:1, while the ratio of crosslinker to chain extender was kept at 1:10. The synthesis procedure was as follows: RM82 (1 g), tetrakis(allyloxy)ethane (0.017 g), and 1,10-Decanedithiol (0.27 g) were dissolved in DMF (1 g) at 80 °C. Next, 0.025 g of DMPA was added to the solution. Then, the LCE solution was immediately injected into the silicone rubber mold, followed by UV curing (365 nm, 200 mW/cm^2) for 3 min. The cured film was then dried in a vacuum oven at 70 °C for 12 h to remove the DMF.

Synthesis of non-acrylate-containing LCE samples

For the non-acrylate-containing epoxy LCE network, the following procedure was used: 1 g of 4,4′-bis(2,3-epoxypropoxy)biphenyl and 0.68 g of sebacic acid were mixed at 180 °C. A triazabicyclodecene catalyst (5 mol% relative to the carboxyl groups) was then added, and the mixture was stirred manually until homogeneous. After cooling to room temperature, the mixture was sandwiched between two glass slides coated with polytetrafluoroethylene tape. The clamped assembly was subsequently heated at 180 °C for 4 h to complete the reaction.

Fabrication of hydrogel indicator

The first step is to prepare a solution containing a mixture of $FeSO_4$ and XO. Dissolve 1 g of $FeSO_4{\cdot}7H_2O$ and 0.05 g of XO in 10 g of deionized water, followed by the addition of 2-3 drops of hydrochloric acid. Stir the mixture thoroughly. The next step is to synthesize the polyacrylamide hydrogel. AAm (1 g) and N, N′-methylene diacrylamide (0.01 g) were dissolved in 5 g deionized water. Then the mixture was added into a 0.6 mm thick mold, followed by UV curing (365 nm, 200 mW/cm^2) for 15 s. After polymerization, the PAAm hydrogel was immediately immersed in a $FeSO_4$-XO mixed solution and allowed to reach a state of swelling equilibrium. Afterward, the hydrogel indicator can be obtained and used immediately.

Orientation fixing process

The APS solution is prepared by dissolving 4 g of APS in 96 g of deionized water. Add a single drop of DBU (0.02 g) to the solution, and mix thoroughly until achieving homogeneity to promote the formation of free radicals. Subsequently, the LCE sample was programmed through the deformation and then immersed in the prepared solution. After allowing it to soak for a designated period, extract the sample and gently blot the surface with a paper towel to eliminate any residual solution. The final LCE actuator will demonstrate reversible deformation capabilities.

Actuation characterization of programmed LCE

The actuation strain for the programmed LCE samples was determined using the formula: actuation strain = $(L_{cold}-L_{heat})/L_{heat} \times 100\%$. Here, L_{cold} and L_{heat} represent the sample lengths at 25 °C and 120 °C, respectively.

Characterization

The polarized optical images were collected using a polarized optical microscope (ECLIPSE E600W POL) at room temperature. The mechanical property was measured using a Zwick/Roell tensile machine at a stretching speed of 10 mm/min at room temperature. The differential scanning calorimetry (DSC) analyses were conducted using a TA Q200 machine at a heating rate of 10 °C/min. The wide-angle X-ray scattering instrument (WAXS, XEUSS 3.0, from XENOCS, France) was employed to determine the orientation of LCE mesogens. The testing parameters were as follows: 70 kV, 3.5 mA, 250 W. The reversible actuation cycle curves were obtained through dynamic mechanical analysis (DMA, controlled stress mode), with a heating/cooling rate of 10 °C/min. Fourier transform infrared spectrometer (FTIR) spectra were conducted using a Nicolet iS50 FTIR spectrometer (Thermo Fisher, USA) with a scanning range from 4000 to 400 cm^{-1}.

Data availability

The authors declare that the data supporting the findings of this study are provided within the article and its Supplementary Information file. Additional data are available upon request from the corresponding author. Source data are provided in this paper. Source data are provided with this paper.

References

1. He, Q. et al. Electrospun liquid crystal elastomer microfiber actuator. *Sci. Robot.* **6**, eabi9704 (2021).
2. Ilton, M. et al. The principles of cascading power limits in small, fast biological and engineered systems. *Science* **360**, eaao1082 (2018).
3. Nie, Z. et al. Light-driven continuous rotating Möbius strip actuators. *Nat. Commun.* **12**, 2334 (2021).
4. Wang, C., Wu, Y., Dong, X., Armacki, M. & Sitti, M. In situ sensing physiological properties of biological tissues using wireless miniature soft robots. *Sci. Adv.* **9**, eadg3988 (2023).
5. Tang, G., Zhao, X., Mei, D., Zhao, C. & Wang, Y. Perspective on the development and application of ionic polymer metal composites: from actuators to multifunctional sensors. *RSC Appl. Polym.* **2**, 795 (2024).
6. Li, G. et al. Self-powered soft robot in the Mariana Trench. *Nature* **591**, 66–71 (2021).
7. Qian, N. et al. A visible and near-infrared light-fueled omnidirectional twist-bend crawling robot. *Adv. Funct. Mater.* **33**, 2214205 (2023).
8. Jiang, Z., Xiao, Y., Cheng, R., Hou, J. & Zhao, Y. Dynamic liquid crystalline networks for twisted fiber and spring actuators capable of fast light-driven movement with enhanced environment adaptability. *Chem. Mater.* **33**, 6541–6552 (2021).
9. Chen, Y., Liu, Q., Theato, P., Wei, J. & Yu, Y. A convenient route to prepare reactive azobenzene-containing liquid crystal polymers and photodeformable fibers. *Adv. Intell. Syst.* **33**, 2000254 (2021).
10. Wang, Y. et al. Repeatable and reprogrammable shape morphing from photoresponsive gold nanorod/liquid crystal elastomers. *Adv. Mater.* **32**, 2004270 (2020).
11. Zhai, F. et al. 4D-printed untethered self-propelling soft robot with tactile perception: Rolling, racing, and exploring. *Matter* **4**, 3313–3326 (2021).
12. Choi, J. et al. Steerable and agile light-fueled rolling locomotors by curvature-engineered torsional torque. *Adv. Sci.* **10**, 2304715 (2023).
13. Huang, Z. et al. Wearable perovskite solar cells by aligned liquid crystal elastomers. *Nat. Commun.* **14**, 1204 (2023).
14. Nie, Z., Wang, M. & Yang, H. Structure-induced intelligence of liquid crystal elastomers. *Chem. Eur. J.* **29**, e202301027 (2023).
15. Herbert, K. M. et al. Synthesis and alignment of liquid crystalline elastomers. *Nat. Rev. Mater.* **7**, 23–38 (2022).
16. Zeng, H., Wani, O. M., Wasylczyk, P., Kaczmarek, R. & Priimagi, A. Self-regulating iris based on light-actuated liquid crystal elastomer. *Adv. Mater.* **29**, 1701814 (2017).
17. Zhang, D. et al. Reversible perspiring artificial "Fingertips". *Adv. Mater.* **35**, 2209729 (2023).
18. Ware, T. H., McConney, M. E., Wie, J. J., Tondiglia, V. P. & White, T. J. Voxelated liquid crystal elastomers. *Science* **347**, 982–984 (2015).
19. Buguin, A., Li, M., Silberzan, P., Ladoux, B. & Keller, P. Micro-actuators: When artificial muscles made of nematic liquid crystal elastomers meet soft lithography. *J. Am. Chem. Soc.* **128**, 1088–1089 (2006).
20. Yao, Y. et al. Programming liquid crystal elastomers for multistep ambidirectional deformability. *Science* **386**, 1161–1168 (2024).
21. Wang, Z. et al. Three-dimensional printing of functionally graded liquid crystal elastomer. *Sci. Adv.* **6**, eabc0034 (2020).
22. Hou, W., Wang, J. & Lv, J. Bioinspired liquid crystalline spinning enables scalable fabrication of high-performing fibrous artificial muscles. *Adv. Mater.* **35**, 2211800 (2023).
23. Kim, I. H. et al. Human-muscle-inspired single fibre actuator with reversible percolation. *Nat. Nanotechnol.* **17**, 1198–1205 (2022).
24. Yue, L. et al. Vacuum thermoforming of optically switchable liquid crystalline elastomer spherical actuators. *Adv. Mater.* **36**, 2402559 (2024).
25. Kotikian, A., Truby, R. L., Boley, J. W., White, T. J. & Lewis, J. A. 3D printing of liquid crystal elastomeric actuators with spatially programed nematic order. *Adv. Mater.* **30**, 1706164 (2018).
26. Saed, M. O. et al. Molecularly-engineered, 4D-printed liquid crystal elastomer actuators. *Adv. Funct. Mater.* **29**, 1806412 (2019).
27. Saed, M. O. et al. Thiol-acrylate main-chain liquid-crystalline elastomers with tunable thermomechanical properties and actuation strain. *J. Polym. Sci. B* **55**, 157–168 (2017).
28. Li, Y. et al. Morphing of stiffness-heterogeneous liquid crystal elastomers via mechanical training and locally controlled photopolymerization. *Matter* **5**, 4332–4346 (2022).
29. Zhao, Y. et al. Twisting for soft intelligent autonomous robot in unstructured environments. *Proc. Natl. Acad. Sci. USA* **119**, e2200265119 (2022).
30. Wang, Y., Sun, J., Liao, W. & Yang, Z. Liquid crystal elastomer twist fibers toward rotating microengines. *Adv. Mater.* **34**, 2107840 (2022).
31. Ohzono, T., Saed, M. O. & Terentjev, E. M. Enhanced dynamic adhesion in nematic liquid crystal elastomers. *Adv. Mater.* **31**, 1902642 (2019).
32. Pei, Z. et al. Mouldable liquid-crystalline elastomer actuators with exchangeable covalent bonds. *Nat. Mater.* **13**, 36–41 (2014).
33. Saed, M. O., Gablier, A. & Terentejv, E. M. Liquid crystalline vitrimers with full or partial boronic-ester bond exchange. *Adv. Funct. Mater.* **30**, 1906458 (2020).
34. Küpfer, J. & Finkelmann, H. Nematic liquid single crystal elastomers. *Die Makromol. Chem., Rapid Commun.* **12**, 717–726 (1991).
35. Yakacki, C. M. et al. Tailorable and programmable liquid-crystalline elastomers using a two-stage thiol-acrylate reaction. *RSC Adv.* **5**, 18997–19001 (2015).
36. Fan, Y. et al. One-step manufacturing of supramolecular liquid-crystal elastomers by stress-induced alignment and hydrogen bond exchange. *Angew. Chem. Int. Ed.* **62**, e202308793 (2023).
37. Wen, Z. et al. Reconfigurable LC elastomers: Using a thermally programmable monodomain to access two-way free-standing

multiple shape memory polymers. *Macromolecules* **51**, 5812–5819 (2018).
38. Chen, G. et al. Rapidly and repeatedly reprogrammable liquid crystalline elastomer via a shape memory mechanism. *Adv. Mater.* **34**, 2201679 (2022).
39. Jin, B. et al. Solvent-assisted 4D programming and reprogramming of liquid crystalline organogels. *Adv. Mater.* **34**, 2107855 (2022).
40. Liang, H. et al. Cloth-to-clothes-like" fabrication of soft actuators. *Adv. Mater.* **36**, 2400286 (2024).
41. Liang, H. et al. Thiol-acrylate catalyst enabled post-synthesis fabrication of liquid crystal actuators. *Chin. J. Polym. Sci.* **41**, 1656–1662 (2023).
42. Lu, L., Leanza, S. & Zhao, R. R. Origami with rotational symmetry: a review on their mechanics and design. *Appl. Mech. Rev.* **75**, 050801 (2023).
43. Filipov, E. T., Tachi, T. & Paulino, G. H. Origami tubes assembled into stiff, yet reconfigurable structures and metamaterials. *Proc. Natl. Acad. Sci. USA* **112**, 12321–12326 (2015).
44. Meloni, M. et al. Engineering origami: A comprehensive review of recent applications, design methods, and tools. *Adv. Sci.* **8**, 2000636 (2021).
45. Felton, S., Tolley, M., Demaine, E., Rus, D. & Wood, R. A method for building self-folding machines. *Science* **345**, 644–646 (2014).
46. Zhou, X. et al. Metal-ligand bonds based reprogrammable and reprocessable supramolecular liquid crystal elastomer network. *Angew. Chem. Int. Ed.* **63**, e202409182 (2024).
47. Silverberg, J. L. et al. Origami structures with a critical transition to bistability arising from hidden degrees of freedom. *Nat. Mater.* **14**, 389–393 (2015).

Acknowledgements

We thank Mrs. Li Xu and Mrs. Sudan Shen for the help of DSC and polarizing microscopy characterizations at State Key Laboratory of Chemical Engineering (Zhejiang University). This work was supported by the National Key R&D Program of China (no. 2022YFB3805701 to J. W.), National Natural Science Foundation of China (no. 52322307 and 22275162 to N. Z.), and Zhejiang Provincial Natural Science Foundation of China (no. LZ25E030007 to N. Z.).

Author contributions

N. Z. and X. Z. conceived the concept. T. X and N. Z. directed the project. X. Z. designed the experiments. X. Z. conducted the experiments. X. Z. and N. Z. wrote the paper. Y. S., G. C., and J. H. analyzed the mechanism. L. L. and H. X. designed the origami pattern. H. W. and Y. W. designed the 3D printing model. H. B., Z. Z., and Q. Z. helped for visualization. J. W. conducted the calculations. All authors discussed the results and contributed to the preparation of the manuscript. All authors have given approval to the final version of the manuscript.

Competing interests

The authors declare no competing interests.

Additional information

Supplementary information The online version contains supplementary material available at https://doi.org/10.1038/s41467-025-62883-8.

Correspondence and requests for materials should be addressed to Ning Zheng.

Peer review information *Nature Communications* thanks Xiaoguang Wang and the other, anonymous, reviewer(s) for their contribution to the peer review of this work. A peer review file is available.

Reprints and permissions information is available at http://www.nature.com/reprints

Publisher's note Springer Nature remains neutral with regard to jurisdictional claims in published maps and institutional affiliations.

Open Access This article is licensed under a Creative Commons Attribution-NonCommercial-NoDerivatives 4.0 International License, which permits any non-commercial use, sharing, distribution and reproduction in any medium or format, as long as you give appropriate credit to the original author(s) and the source, provide a link to the Creative Commons licence, and indicate if you modified the licensed material. You do not have permission under this licence to share adapted material derived from this article or parts of it. The images or other third party material in this article are included in the article's Creative Commons licence, unless indicated otherwise in a credit line to the material. If material is not included in the article's Creative Commons licence and your intended use is not permitted by statutory regulation or exceeds the permitted use, you will need to obtain permission directly from the copyright holder. To view a copy of this licence, visit http://creativecommons.org/licenses/by-nc-nd/4.0/.

© The Author(s) 2025